ADVANCED HEALTHCARE MATERIALS
www.advhealthmat.de

Novel Multifunctional Meta-Surface Plasmon Resonance Chip Microplate for High-Throughput Molecular Screening

Youqian Chen, Huazhi Zhang, Rui Li, Hongli Fan, Junjie Huang, Rui Zhou, Shaoping Yin, Gang L. Liu,* and Liping Huang**

The utilization of surface plasmon resonance (SPR) sensors for real-time label-free molecular interaction analysis is already being employed in the fields of in vitro diagnostics and biomedicine. However, the widespread application of SPR technology is hindered by its limited detection throughput and high cost. To address this issue, this study introduces a novel multifunctional MetaSPR high-throughput microplate biosensor featuring 3D nanocups array structure, aiming to achieve high-throughput screening with a reduced cost and enhanced speed. Different types of MetaSPR sensors and analytical detection methods have been developed for accurate antibody subtype identification, epitope binding, affinity determination, antibody collocation, and quantitative detection, greatly promoting the screening and analysis of early-stage antibody drugs. The MetaSPR platform combined with nano-enhanced particles amplifies the detection signal and improves the detection sensitivity, making it more convenient, sensitive, and efficient than traditional ELISA. The findings demonstrate that the MetaSPR biosensor is a new practical technology detection platform that can improve the efficiency of biomolecular interaction studies with unlimited potential for new drug development.

1. Introduction

The necessity of rapid and precise real-time, label-free molecular interaction analysis cannot be overstated, particularly in the context of drug screening[1] and early diagnostics.[2] Significant advancements have been achieved in molecular interaction measurement techniques in recent years, specifically within the label-free domain. Prominent examples of such methodologies include mass spectrometry, surface plasmon resonance (SPR), biolayer interferometry (BLI), and backscattering interferometry. These approaches facilitate the detection and determination of molecular interactions without altering the constituents involved.[3]

Commonly used label-free molecular interaction systems in the field encompass BLI, SPR,[4] and local surface plasmon resonance (LSPR).[5] These methodologies are utilized for the prompt, label-free, and efficient detection of molecular interactions. However, high instrument and material costs, large size of equipment, and high technical requirements for operators hinder the widespread use of these methods in scientific research institutions, small pharmaceutical companies, and other research environments with limited resources. BLI devices based on these technologies, such as ForteBio's eight-channel instrument, are unsuitable for general laboratories because of their relatively low sensitivity, high price, and expensive reagents. Traditional SPR systems, exemplified by the commercially available Biacore system, are widely regarded as the benchmark for molecular affinity detection.[6] Nevertheless, the Biacore system necessitates the utilization of a coupling prism device or alternative apparatus to induce photon excitation and replicate SPR phenomena. The intricate configuration of the Biacore system, coupled with the exorbitant expenses associated with procuring imported instrument components,[7] restricts the extensive adoption of this system

Y. Chen, R. Li, H. Fan, G. L. Liu, L. Huang
College of Life Science and Technology
Huazhong University of Science and Technology
Wuhan 430074, China
E-mail: loganliu@hust.edu.cn; lphuang@aliyun.com

H. Zhang, R. Zhou, G. L. Liu, L. Huang
Biosensor R&D Department
Liangzhun (Wuhan) Life Technology Co., Ltd.
Wuhan 430070, China

J. Huang
College of Life Science and Technology
Wuhan University of Bioengineering
Wuhan 430400, China

S. Yin
School of Pharmacy
Jiangsu Provincial Engineering Research Center of Traditional Chinese Medicine External Medication Development and Application
Nanjing University of Chinese Medicine
Nanjing 210023, P. R. China
E-mail: ysp0305@126.com

S. Yin
State Key Laboratory of Natural Medicines
Department of Pharmaceutics
China Pharmaceutical University
Nanjing 210009, P. R. China

The ORCID identification number(s) for the author(s) of this article can be found under https://doi.org/10.1002/adhm.202401097

DOI: 10.1002/adhm.202401097

across various domains. Although LSPR systems are conveniently and economically designed, they exhibit low sensitivity, poor stability, and low repeatability of results. Thus, highly specific, portable, and affordable technologies that can be widely used in molecular interaction analysis are urgently required.

The nanocup microarray MetaSPR is based on the principle that when the surface structure of a nano-metal is irradiated by incident light, metal-free electron resonance is induced, which causes the emission of secondary light and the formation of a specific absorption spectrum. Changes in the molecules or solutions on the chip surface alter the intensity of the transmitted plasmon resonance light at specific wavelengths (595 and 575 nm for the chips used in the experiment). The transmitted wavelength before the shift is then subtracted from that after the shift, resulting in a significant decrease in light intensity at 575 nm and an increase at 595 nm. Therefore, the interactions between biomolecules can be analyzed based on changes in the absorption intensity of the two wavelengths during the reaction. The factors that primarily determine the wavelength are the nanostructure size,[8] the deposited metal layer,[9] and the metal layer thickness.[10] 3D nanocup microarray chips are a key factor in improving detection performance.[11] The relationship between the interface structure and enhanced detection performance has been reported in our previous study. For Instance, Ameen et al.[12] have reported a sensor design and sensing method based on plasmonic–photonic interactions that occur when a nanocavity array is embedded in a 3D tapered nanocup plasmonic substrate. This device enables the highly sensitive detection of refractive index changes based on modifications to the transmission peak intensity without a shift in the resonance wavelength. Unlike conventional plasmonic sensors, there is a consistent and selective change in the transmission intensity at the resonance peak wavelength with no spectral shift. Zhang et al.,[13] optimized the Ti-Au chip based on this chip structure, and a digital plasma immunosorbent assay, based on a nanopore biosensor, is presented. This method is highly sensitive for detecting low protein concentrations. Meanwhile, Li et al. compared the size of the nanocup, determined the optimal nanocup size, and proposed a vaporized Ti-Ag-Au chip based on the optimal nanostructure.[8] This improved chip has an RI of 759.50 nm/RIU and an FOM of 23.01. These studies have greatly improved the detection performance of nanocup microarray structured chips.

In our previous study, we showed that a MetaSPR sensor with a nanopore array could detect affinity by monitoring the correlation process.[14] The metal periodic nanostructure sensors are stimulated by light to induce collective oscillations of the electron gas, resulting in a decrease in the intensity of reflected light without the need for coupling devices. Given this detection principle, MetaSPR presents itself as a highly suitable option for emerging SPR laboratories.[15] Despite its numerous advantages, MetaSPR technology is predominantly employed in the quantification of the concentrations of various biomarkers. We earlier showed that the MetaSPR chip biosensor has unique optical properties owing to its uniform nanocup structure, thus indicating the feasibility of generating an easy-to-use MetaSPR molecular interaction desktop instrument that meets the requirements of individuals and laboratories.[16]

MetaSPR is fundamentally different from traditional SPR regarding technical principles. Traditional SPR, with sensors based on glass, analyzes the strength of molecular interactions by recording changes in the angle of the resonance peak offset, while MetaSPR technology, whose sensors are based on PET, reacts to intermolecular interactions through changes in the size of the resonance peak displacement. Therefore, although the molecular interaction methodologies of the two technologies are similar, they use different technology platforms, and the operation of their practical applications is distinct. Specifically, the chip sensor types and the modification and manipulation methods are also different. SPR facilitates a dynamic process of molecular binding and dissociation through the use of microfluidics. In contrast, MetaSPR achieves a similar dynamic process via high-speed vibration and liquid exchange, a methodology akin to existing BLI molecular interaction platforms. Molecular interactions in the MetaSPR and systematic studies on subtype identification, epitope binding, or antibody screening have not been analyzed in detail since its development,[17] although there are reports on quantitative detection[10,18] and affinity evaluation.[8,16] This study provides a systematic research basis for MetaSPR technology and lays a methodological foundation for drug screening through the development of applications, which is innovative and groundbreaking from a methodological point of view.

In this study, a wafer-scale 3D nanocups array chip was produced, biochemically modified to fabricate the MetaSPR chip sensors, and integrated onto 3D-printed bottomless 96- and 384-well plates to achieve high-throughput detection assays with 96-throughput detection or 384-throughput detection. A portable affinity analysis device was then assembled by combining the 96- and 384-throughput biosensor with an optical signal-detection device and powerful data-computing system, which expands the application of MetaSPR for high-throughput drug screening (**Figure 1a**). The 96-well plate was used for 96-throughput and the 384-well plate for 384-throughput. This reflects the high-throughput attributes of the platform. Based on this high-throughput screening platform, three molecular interactions are proposed to launch a series of applications. The MetaSPR chip sensor detects interactions between different molecules, such as subtype identification, affinity evaluation, epitope binding, antibody collocation, and quantitative detection, by monitoring changes in light intensity at certain wavelengths, which can produce stable detection results within 15 min. In addition, the detection sensitivity of the developed MetaSPR platform combined with gold nanoparticles (AuNPs) was further improved by one to two orders of magnitude (Figure 1b). We also established various MetaSPR biosensors using different modification methods to validate the interactions between different biomolecules. The developed MetaSPR platform has high-throughput, high-sensitivity, and low-cost characteristics, making it promising for applications in drug screening and drug discovery.

2. Results and Discussion

2.1. Establishment of a Detection Method Based on the MetaSPR Sensor

In this study, we developed three analytical detection methods (direct capture, sandwich, and competition) to immobilize antigens or antibodies on the surface matrix of the MetaSPR 3D nanocups array sensor chip via covalent binding, charge adsorption,

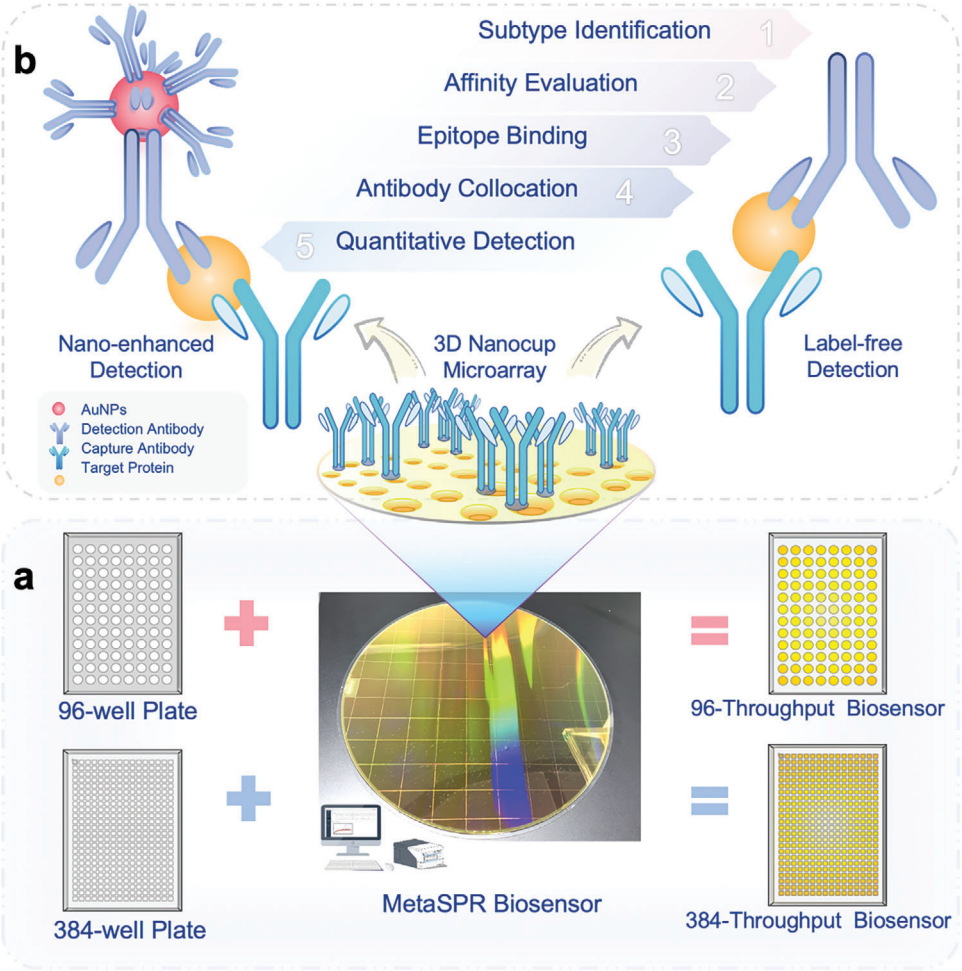

Figure 1. Schematic diagram of the MetaSPR chip sensor platform for molecular interaction detection. a) A convenient high-throughput biosensor. b) The principle of molecular interactions based on the MetaSPR sensing platform and the research of five applications.

hydrophilicity, hydrophobicity, gold sulfur bonding, and other principles to analyze biomolecular interactions (**Figure 2**).

The direct capture method is utilized for conducting epitope grouping, affinity determination, and subtype identification, as well as for directly analyzing intermolecular interactions. The specific principle underlying affinity determination is illustrated in Figure 2a. In this approach, the ligands are immobilized on the chip, and label-free analytes (or antibodies) are subsequently detected. If the antigen binds to the antibody, the binding curve exhibits an upward trajectory; conversely, if no binding occurs, the binding curve remains unchanged (Figure 2b). Based on this principle, the direct capture method can also be utilized for antibody subtype identification. This process involves fixing the secondary antibody on the chip surface, binding it with specific antibodies, and distinguishing the antibody subtypes.

The sandwich method is applicable for various purposes such as antibody collocation, epitope binding, protein quantification, and other applications. Figure 2c provides an illustration of the principle underlying the sandwich method, wherein the antibody is immobilized on the MetaSPR chip surface and subsequently binds to the antigen. Subsequently, a secondary antibody is introduced to form an antibody-antigen-antibody complex. Furthermore, by employing signal amplification techniques, gold-particle-labeled antibodies enable the quantitative or qualitative detection of complex viral samples.[18b] The sandwich method commonly enhances the signal of the secondary antibody through the utilization of horseradish peroxidase[10] or gold particle labeling,[18e] thereby elevating the binding curve of the secondary antibody. If the second antibody fails to bind, the real-time curve will exhibit no upward trend (Figure 2d).

The competition method can be employed for epitope grouping, quantitative detection and specific antibody analysis, as well as other assays. For example, the principle of the epitope binding is shown in Figure 2e, wherein, the antibody is immobilized on the surface of the MetaSPR chip, and the antibodies awaiting competition and antigen are premixed until antigen binding is saturated. Then, complexes of competitive antibodies and antigens are simultaneously added to the chip. If both antibodies bind to the same epitope, the binding is blocked and the binding curve becomes flat. If the two antibodies bind to different epitopes, then blocking will not occur, and the binding curve will show an upward trend (Figure 2f).

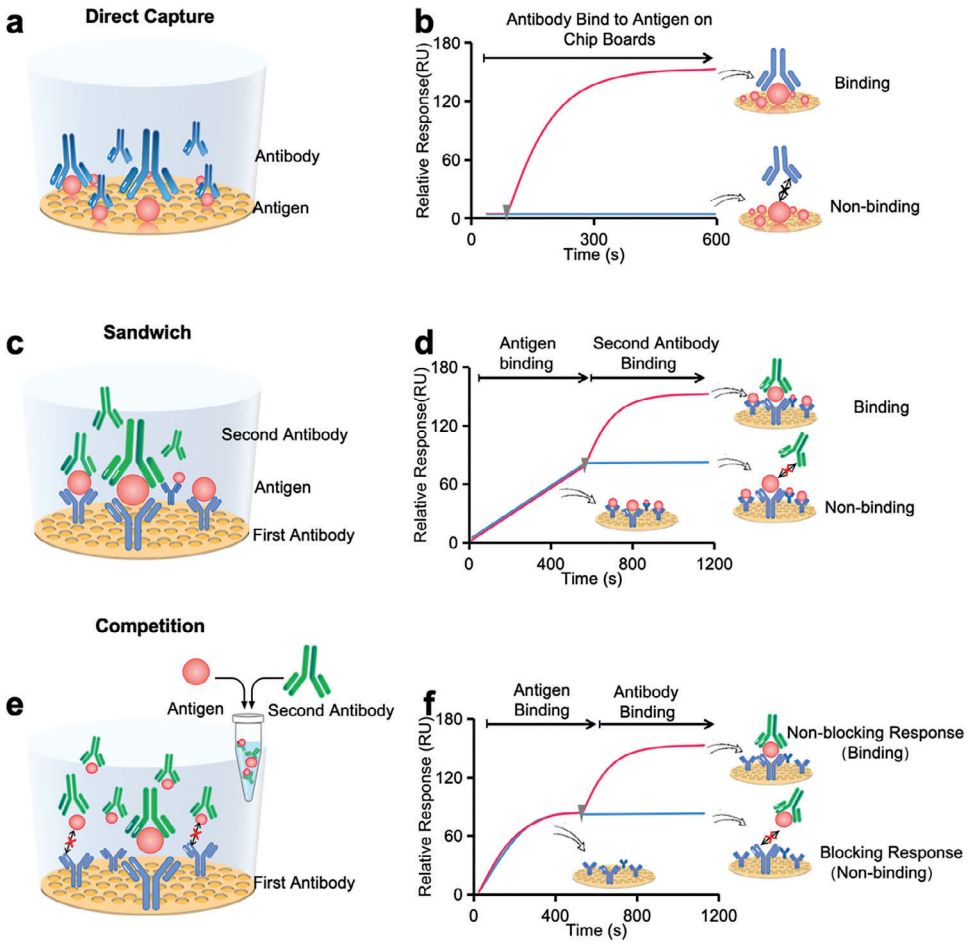

Figure 2. Schematic illustration of the principles underlying the three analytical detection methods. a) Direct capture detection. b) Addition sequence and binding effect of the molecular interactions determined using direct capture detection. c) Principle of sandwich detection. d) Addition sequence and binding effect of the molecular interactions determined using sandwich detection. e) Principle of competition detection. f) Addition sequence and binding effect of the molecular interactions determined using direct capture detection.

2.2. Surface Characterization of the MetaSPR Chip

Periodic nanocup array sensor chips were fabricated on polymer substrates with nanocup microarray structures. **Figure** 3c depicts a photograph of the chip, showcasing the multicolor light effect, which serves as evidence of the chip sensor's heightened sensitivity. The nanocup array exhibited high uniformity as shown by atomic force microscopy (AFM) (Figure 3a,b), indicating good chip consistency. Most label-free methods that immobilize one of the interacting molecules on a sensor surface (such as BLI and SPR) rely on the refractive index (RI). The microarray nano gold chip's surface exhibited distinct colors due to the presence of two distinct refractive indices, namely air (RI = 1.00027) and water (RI = 1.3330), thereby indicating the chip's exceptional detection sensitivity (Figure 3d). To further substantiate this finding, the absorption spectra of sucrose solutions with varying concentrations, corresponding to RI values ranging from 1.3330 to 1.4062, were measured using a conventional microplate reader. The findings of this study demonstrated that as the concentration of sucrose increased and the RI increased, the peak wavelengths exhibited a gradual red-shift (Figure 3e). Additionally, there was a decrease in light intensity at ≈575 nm and an increase at ≈595 nm (Figure 3e). Because of the red-shift phenomenon, when the absorption spectrum of sucrose is subtracted from that of water to obtain the displacement difference spectrum (Figure 3f), there are negative response units at 575 nm and positive response units at 595 nm. Moreover, as the RI increases, the greater the change in RI, the more pronounced the trough at 575 nm, and the peak at 595 nm become. The difference between the optical density at these two wavelengths (OD_{595}–OD_{575}) exhibited a strong linear correlation with the RI value, suggesting that the chip possessed the capability to detect a change in RI of 0.0005 (Figure 3g). The linear regression analysis of eight data points showed a high R^2 value of 0.9946, signifying a strong linear correlation (Figure 3h). These alterations in surface characteristics were also corroborated by Fan et al.,[16] thus confirming the high detection sensitivity of the MetaSPR chip.

When performing MetaSPR experiments using gold chips, to ensure the accuracy and reproducibility of the signals, the gold chip surface needs to be cleaned. The microarray chip was

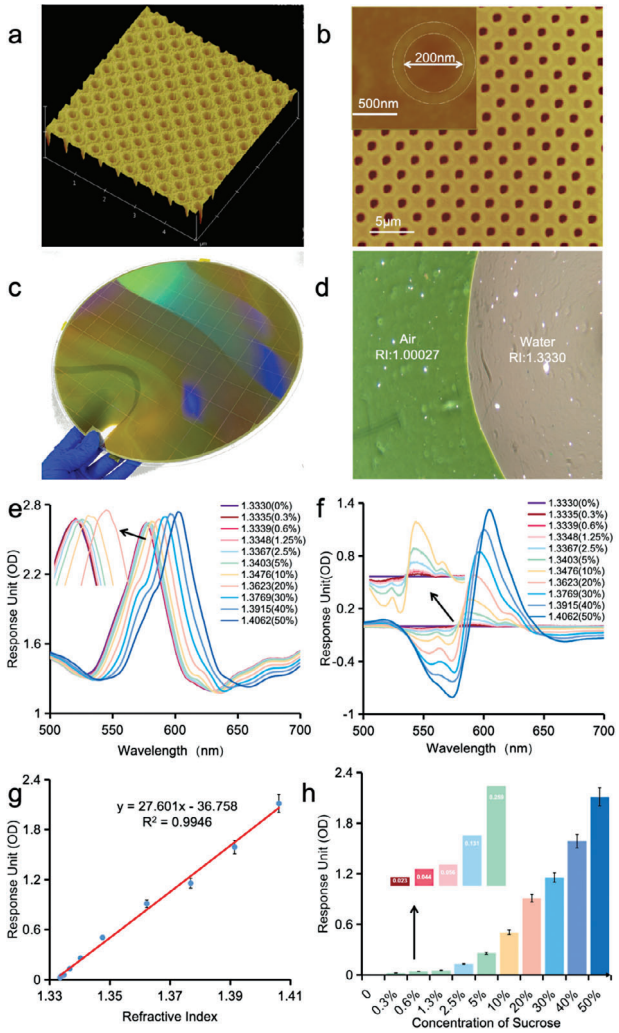

Figure 3. Surface characterization of the chip. a) 3D surface feature map view of the scanning chip determined using AFM microscopy. b) The surface of Meta SPR chips was characterized using AFM analysis. c) A photograph depicting the MetaSPR chip is presented. d) The chip's surface exhibits a green color in the air and turns pink when submerged in water. e) To determine absorption values, a gradient diluted sucrose concentration ranging from 0% to 50% was employed, with a refractive index (RI) range of 1.3330 to 1.4062. The absorption spectrum is subject to variations in RI. f) Differential spectra of sucrose solutions with varying concentrations were obtained after zeroing. g) A strong positive correlation coefficient of 0.9948 is observed between the differences in dual-wavelength optical density (OD) values. Data represent as mean ± SD ($n = 3$). h) The MetaSPR chip exhibits varying dual-wavelength OD differences (OD595-OD575) in response to sucrose solutions with different refractive indices. Data are shown as mean ± SD ($n = 3$).

cleaned with NaOH solution, HCl solution, ethanol solution,[19] and ddH_2O sequentially before any chemical modification. Chip cleaning can remove organic contaminants and impurities such as dust on the gold chip surface. The dried clean chips were directly used as sensors for SPR detection or were chemically modified to create functional chip sensors. The chips were placed under vacuum to avoid surface oxidation. The affinity and selectivity of the molecules on the gold chip surface increased following chemical modification of the MetaSPR gold chip surface, such as the addition of carboxyl and amino groups, which were beneficial for altering and controlling the adsorption, orientation, and stability of biomolecules because of changes in the surface charge and hydrophilicity.

2.3. Applications of MetaSPR Chip

2.3.1. Application 1: Subtype Identification

Identifying antibody subtypes is extremely important in biological research and clinical medicine.[20] Antibody subtype identification can help determine antibody function and antigen-binding specificity.[21] In clinical settings, antibody subtype identification facilitates the diagnosis and treatment of various diseases. For example, in certain autoimmune diseases, the production of specific antibody subtypes is closely associated with disease initiation and progression.[22] Antibodies of a certain subtype, which bind to secondary antibodies with much higher specificity relative to other antibodies that have not been subtyped identified. The five main immunoglobulin classes are IgG, IgM, IgA, IgD, and IgE.[23]

To determine the mouse antibody subtypes, the binding of specific antibodies to mouse IgG1-, IgG2a-, and IgG2b was determined using a carboxylation MetaSPR sensor. Chemical modification can introduce chemical functional groups on the surface of the gold chip, increasing the affinity and selectivity of molecules. For example, functional groups such as carboxyl and amine groups can be introduced onto the surface of gold chips to further modify and control the adsorption, orientation, and stability of biomolecules. In addition, chemical modification can regulate physicochemical properties such as charge and hydrophilicity on the surface of gold chips, which can further improve the adsorption and detection performance of biomolecules. Mercaptoundecanoic acid (MUA) is the first choice for surface modification because it contains sulfhydryl and carboxylic groups that can attach to the gold surface and bind to the amino groups of proteins. The conditions were optimized based on a published MUA surface functionalization method to improve the detection sensitivity of the 3D nanocup microarray gold-chip sensor platform.[15a] Chip performance was improved by a combination of alcohol washing and chemical modification, which further enhanced the sensitivity, signal-to-noise ratio, repeatability, and stability of the SPR experiments. Specific proteins can also be attached to 2D[24] or 3D[12] modified chips to form biosensors to capture specific antibodies or proteins.

A block of the subtyping assay chip sensor can directly distinguish the subtype of the tested antibody within 10 min using the direct capture method. The principle and detection process for subtype screening using the MetaSPR chip sensor are shown in **Figure** 4a. The secondary antibodies specific to mouse IgG1, IgG2a, and IgG2b were immobilized on the carboxylation MetaSPR sensor in columns one to three, followed by blocking of the non-specific binding sites. The antibody to be tested was added to the microplate wells, and if the antibody was bound to a specific rabbit anti-mouse IgG1 antibody, the subtype of the

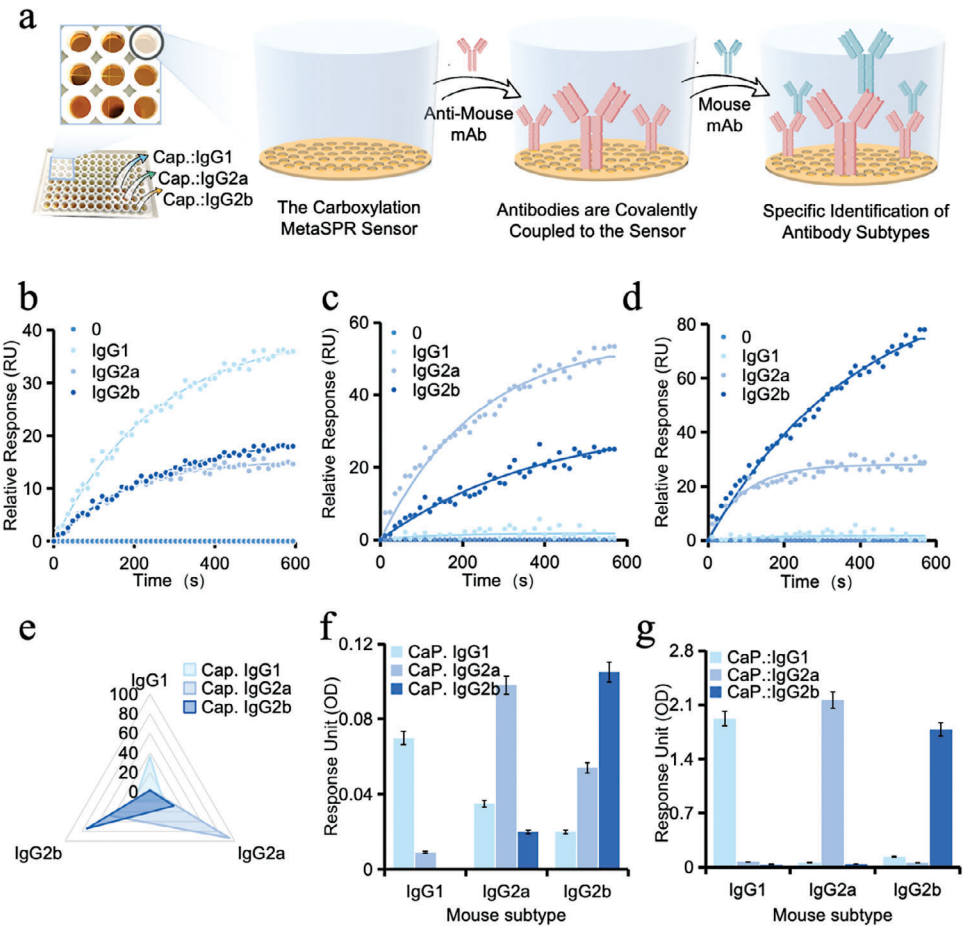

Figure 4. Subtype identification analysis. a) Schematic diagram of the subtype identification and detection process and principle. b) Rabbit anti-mouse IgG1, c) IgG2a, and d) IgG2b antibodies were fixed on the carboxylation MetaSPR sensor chip, and mouse IgG1, IgG2a, and IgG2 antibodies were detected real-time. e) MetaSPR subtype identification. f) Relative response at 575 and 595 nm before and after subtype identification on the surface of the sensor chip. Data represent as mean ± SD ($n = 3$). g) Results of subtype identification using ELISA. Data represent as mean ± SD ($n = 3$).

tested antibody was determined as IgG1. Using parity of reasoning, the light-chain subtype could also be measured. The relative responses of IgG1, IgG2a, and IgG2b are shown in Figure 4b–d, respectively. The strongest binding to rabbit anti-mouse IgG1, rabbit anti-mouse IgG2a, and rabbit anti-mouse IgG2b antibodies was observed in the IgG1, IgG2a, and IgG2b subtypes, respectively (Figure 4e). Within a 10-min timeframe, a change in the response unit proportional to the different IgG subtypes was detected at 595 nm in the typical differential absorption spectrum (Figures S1–S3, Supporting Information)[10] of the MetaSPR sensor chip (Figure 4f). We then compared the MetaSPR chip sensor screening result with traditional ELISA screening result (Figure 4g, Table S1, Supporting Information) and found that the results of subtype identification from the two methods were consistent. This explains the accuracy of the identification results. However, ELISA requires at least 1.5 h of incubation-washing-color development-termination to obtain results, while the Meta SPR platform assay requires only 10 min of association with the addition of the antibody to be tested, and the result can be obtained in one step. This greatly improves the efficiency of the assay. Furthermore, compared with traditional SPR's single-needle liquid-phase injection, MetaSPR uses a 96-well plate assay, which can detect 96 wells at the same time, so the throughput is higher than that of traditional SPR. Thus, the MetaSPR sensing platform is able to quickly identify antibody subtypes in one step, being a quick and high-throughput method.

2.3.2. Application 2: Affinity Evaluation

Affinity is a measure of the intensity of the interactions between two molecules in a reversible reaction. Affinity-based protein interaction evaluation has applications in diverse domains, including early-stage drug investigation, screening and identification, preclinical and clinical research, and downstream production quality control. In preclinical studies, the evaluation of protein interaction affinity has been extensively employed to investigate the underlying mechanisms of signaling pathways. Ligand-binding interactions play a crucial role in maintaining the native conformation of proteins. Since protein G binds to the Fc region of an antibody and can bind to IgG with high affinity,[25] it was immobilized onto the chip surface to form a protein G sensor. This sensor can be used for antibody concentration quantification and biomolecular interaction evaluation.

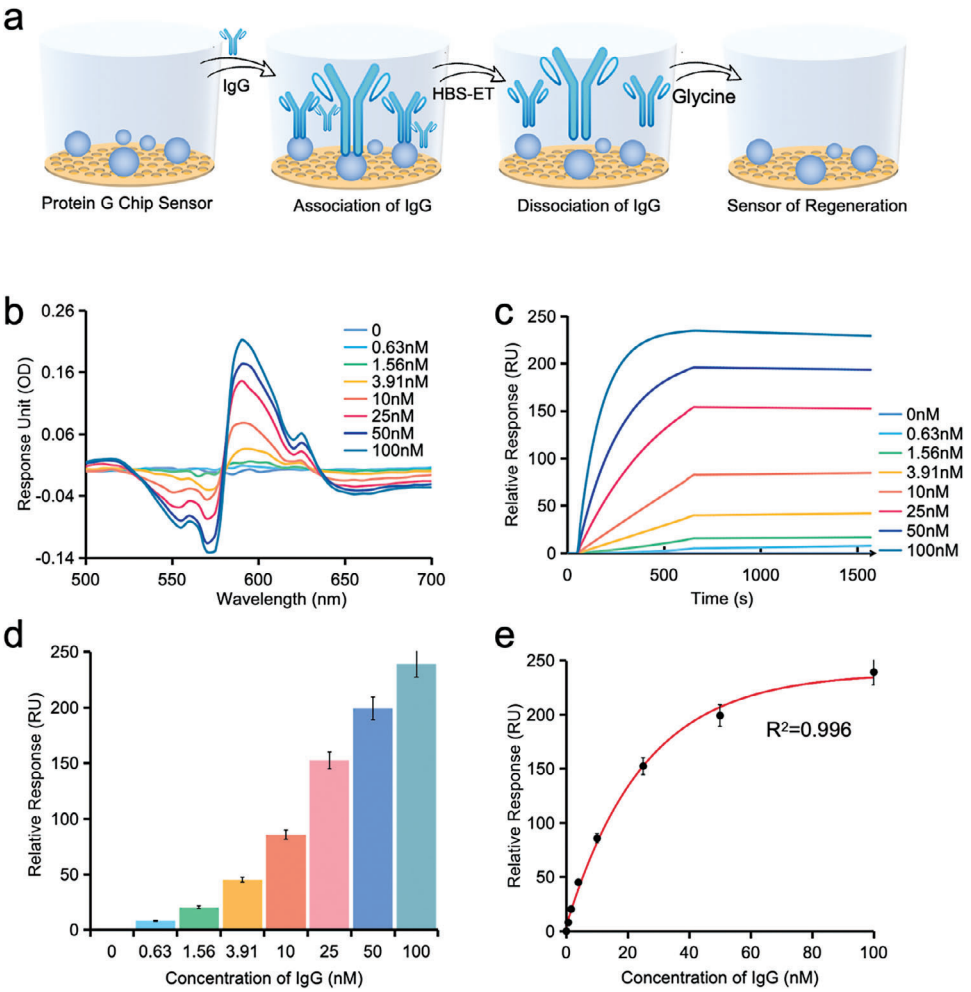

Figure 5. Affinity evaluation based on the MetaSPR sensor. a) Schematic diagram of the protein G-IgG affinity evaluation principle. b) Differential spectra at 575 and 595 nm after IgG binding to protein G. c) Kinetic fitting curves derived from the association and dissociation data of protein G and IgG, encompassing a range of analyte concentrations from 0 to 100 nM. d) Relative response difference between serial dilutions of IgG. Data represent as mean ± SD ($n = 3$). e) Correlation of the relative response difference between serial dilutions of IgG, $R^2 = 0.996$. Data represent as mean ± SD ($n = 3$).

This study established a protein G-IgG interaction platform based on affinity evaluation using direct capture method (**Figure** 5a), which can simultaneously detect and create the binding and dissociation curves in a high-throughput manner. During the detection process, the protein G chip wells were subjected to the addition of diluted IgG at concentrations ranging from 0.63 to 100 nM. Following the association period of 10 min, the sample was dissociated using a diluent, as depicted in Figure 5c. This was done to create a convenient and rapid high-throughput binding and dissociation kinetic assay. Figure 5b illustrates the determination of the change in optical density (OD) at a specific wavelength after the addition of diluted IgG samples at various concentrations to the chip. The real-time dynamic binding curves of the IgG samples at 595 and 575 nm yielded a dual-wavelength relative response difference of 600 s, as shown in Figure 5d.

The standard curve depicting the dual-wavelength relative response difference in relation to the IgG concentration (ranging from 0.63 to 100 nM) is presented in Figure 5e. A four-parameter logistic regression model was employed to generate the standard curve, yielding an R^2 value of 0.996, which shows a strong linear correlation. To account for variability, each data point on the graph is each data point in the graph represents the mean of three separate experiments, ensuring a more accurate depiction of potential fluctuations. Subsequently, the affinity between Protein G and IgG was assessed. Exponential functions of the form $y = a\ (1 - e^{-bx})$ were fitted to the plots shown in Figure 5c. The values of the association rate constant (Ka) and the dissociation rate constant (Kd) were determined as 9.66×10^6 M^{-1} s^{-1} and 6.14×10^{-5} s^{-1}, respectively. According to the calculations from the constants of intermolecular interactions, the affinity constant (KD) between Protein G and IgG was 6.11×10^{-10} M (611 pM) (the dynamic processes of molecular interactions, and the methods to determine the constants of intermolecular interactions as shown in Table S2, Supporting Information). Notably, the obtained KD value was found to be similar to previous reports.[25] Additionally, the analysis of kinetic fitting curves derived from the association and dissociation data of protein G and IgG further supports its utility. Hence, the MetaSPR biosensor device exhibits considerable potential as a high-throughput screening platform in

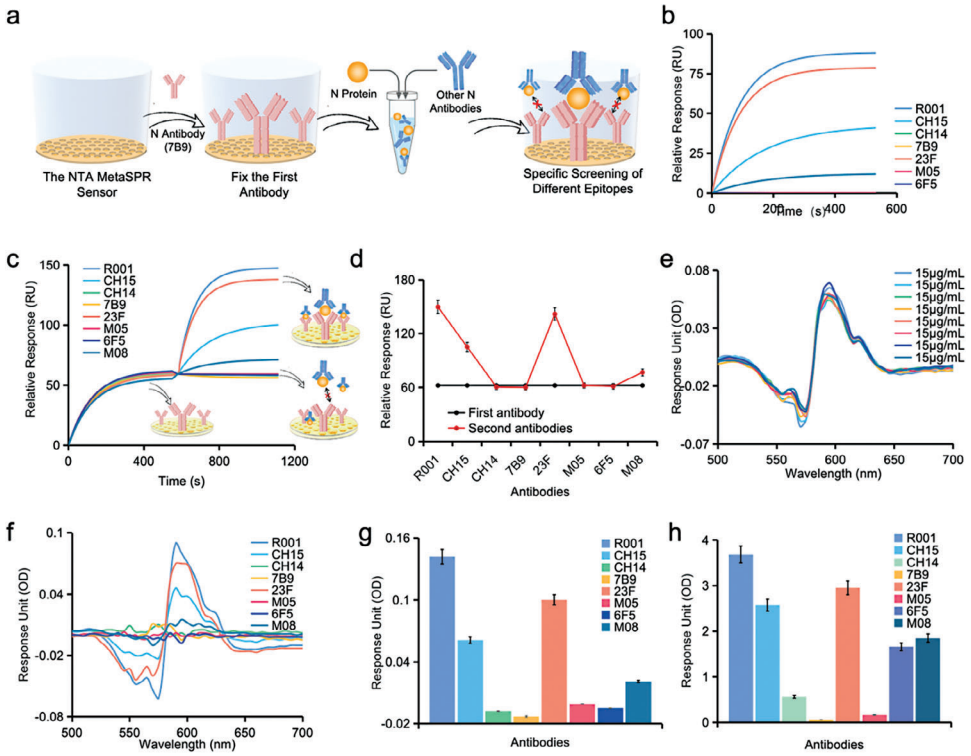

Figure 6. Epitope binding determined using the MetaSPR sensor. a) Epitope identification: NTA chip sensor coupled with the SARS-CoV-2 nucleoprotein antibody (7B9); the SARS-CoV-2 nucleoprotein protein was incubated with different SARS-CoV-2 nucleoprotein specific antibodies, which competed with the SARS-CoV-2 nucleoprotein protein-specific antibody conjugated on the chip. b) Relative response curve of the nucleoprotein pre-saturated with the second followed by binding with the antibody conjugated on the chip. c) Relative response of the nucleoprotein-specific antibodies binding to different epitopes, as identified by the dual antibody sandwich method. d) Identification results of antibodies with different epitopes than antibody 7B9. The epitopes bound by antibody 7B9 were different from those of R001 and 23F and were the same as those of CH14, M05, and 6F5. Data represent as mean ± SD ($n = 3$). e) Differential spectra at 575 and 595 nm after antibody 7B9 was conjugated onto the chip. f) Differential spectra at 575 and 595 nm after different antibodies bound to the nucleoprotein and antibody 7B9 on the MetaSPR sensor. g) Histogram of the two-wavelength response unit showing differences in antibodies with different epitopes relative to 7B9. Data represent as mean ± SD ($n = 3$). h) Results of ELISA-based epitope identification. Data represent as mean ± SD ($n = 3$).

laboratory settings, enabling convenient, label-free, and efficient quantification of antibody concentrations and affinity assays.

2.3.3. Application 3: Epitope Binding

Multiple antibody-binding epitopes facilitate the screening of antibodies from paired antibodies and natural samples, which directly improves the success rate of the pairing.[26] The epitope directly determines antibody specificity. If the target epitope of an antibody is relatively concentrated and steric hindrance is large, then the success rate of pairing will be affected.[27] The identification of epitopes, which are the specific regions on an antigen that interact with antibodies, plays a crucial role in the development of antibody-based drugs.[28] Epitope binding, a widely utilized technique involving the analysis of polyclonal antibodies in immunized animals' sera, is instrumental in the discovery of antigenic components of pathogens. This process yields invaluable insights that aid in the development of vaccines and therapies.[29] However, it is important to note that epitopes capable of binding to multiple antibodies may exhibit cross-reactivity with various antibodies and non-target molecules. Consequently, the precise identification of specific epitopes assumes paramount significance.

In this study, a nitrilotriacetic acid (NTA)-based MetaSPR sensor was selected for epitope identification using the competition method. Nickel binds to the His-tag, thereby facilitating the analysis of His-tagged proteins and interacting molecules. The detection process is shown in **Figure 6**a. The chip was conjugated with SARS-CoV-2 N antibody (7B9). Next, SARS-CoV-2 N protein (RM1033; 10 μg mL^{-1}) was premixed with eight SARS-CoV-2 N antibodies from different manufacturers and added into the chip well to screen antibodies binding to different epitopes of the N antibody 7B9. When the N antibody 7B9 was conjugated onto the chip, differential spectra were noted at 575 and 595 nm (Figure 6e), which showed that the MetaSPR chip had extremely high consistency. The epitopes of the SARS-CoV-2 N proteins that bound with the N antibodies from different manufacturers and the N antibody 7B9 conjugated on the chip differed (Figure 6d). Moreover, the epitopes of each of the tested antibodies differed as shown by the differential spectra at 575 and 595 nm (Figure 6f).

In the amalgamation of the two segments, antibody R001 exhibited a greater affinity, suggesting that antibodies R001 and 7B9 possessed distinct epitopes (Figure 6c). The combination of

Table 1. Comparison of epitope identification using MetaSPR and ELISA. From top to bottom, the sequences ranged from epitopes different from those for 7B9 to the same epitope as for 7B9.

Ranking	MetaSPR ranking	ELISA ranking
Different epitope	R001	R001
↓	23F	23F
Same epitope	CH15	CH15
	M08	M08
	6F5	6F5
	CH14	CH14
	M05	M05
	7B9	7B9

the initial and subsequent segments demonstrated the most pronounced relative response, followed by 23F. Remarkably, CH14, 7B9, M05, and 6F5 displayed minimal binding with 7B9, indicating the congruity of their epitopes (Figure 6d). The disparity in epitopes is manifested through the discrepancy in the dual wavelengths (Figure 6g). The findings of this study demonstrate that 7B9 exhibits distinct binding epitopes with R001, displaying partial similarity to CH15, 23F, and M08, while displaying nearly identical binding epitopes with CH14, 6F5, and M05 (Figure 6g). Furthermore, the conventional ELISA results (Figure 6h) corroborate the dissimilarity in epitopes between R001 and 7B9, aligning with the outcomes of the MetaSPR epitope screening (**Table 1**).

2.3.4. Application 4: Antibody Collocation

In the realm of drug development, the necessity for antibodies that exhibit binding to a wide range of epitopes is frequently observed, as it enhances the likelihood of discovering potential candidates possessing distinct pharmacological characteristics.[30] To effectively apply these approaches in a clinical context, it is imperative to conduct a comprehensive examination of the underlying mechanisms governing the interaction between affinity ligands and their target molecule, along with an assessment of the functional ramifications resulting from this interaction.[31] The process of epitope identification plays a crucial role in determining whether various antibodies exhibit binding to identical epitopes. In addition, an optimal antibody pair can be screened using the MetaSPR label-free system to verify antibody pairs binding to different epitopes.

Our findings indicate that M08, R001, 7B9, CH15, and 23F exhibit binding to distinct epitopes. **Figure 7a** illustrates the underlying principle and procedure of detecting SARS-CoV-2 through antibody-pairing using the sandwich method. Each of these antibodies was individually immobilized on the MetaSPR sensor surface coated with growing gold seeds, followed by incubation with the nucleocapsid protein. Subsequently, the binding of the remaining four antibodies was assessed. A negative control was established using buffer. Through this analysis, we identified the antibody pair that displayed the highest level of responsiveness as the optimal choice. The results of the collocation analysis demonstrated that M08, when conjugated on the MetaSPR sensor surface, exhibited binding affinity toward the nucleocapsid protein, as evidenced by a response value of 62RU. Furthermore, among the four remaining antibodies tested in the subsequent step, 23F displayed the highest relative response, suggesting that M08 and 23F could potentially serve as a compatible antibody pair (Figure 7b). Similarly, 7B9 was found to be the most suitable candidate for pairing with R001 (Figure 7c). The capture antibody 23F was utilized, and the detection antibody 7B9 exhibited the highest level of responsiveness (Figure 7d). Conversely, when the capture antibodies 7B9 and CH15 were employed, the detection antibody 23F displayed the greatest degree of responsiveness (Figure 7e,f), thereby indicating their compatibility as paired antibodies.

Figure 7g shows the comparison of the response values of different antibodies binding the same concentration of N protein after the chip was immobilized with different antibodies. The examination of the binding efficacy of the five antibodies as capture antibodies demonstrated that R001 exhibited the most robust binding, with a relative response of 78RU (Figure 7g). That is, R001 is most suitable to be immobilized on the chip surface as a capture antibody. Furthermore, among the detected antibodies, 7B9, M08, and CH15 exhibited favorable binding capabilities with the nucleocapsid protein (Figure 7h,i) shows the results of different antibodies used as capture antibodies to detect different detection antibodies, and the examination of the relative response of antibody pairs targeting the nucleocapsid protein demonstrated that the combination of R001 as the captured antibody and 7B9 as the detected antibody yielded the highest overall relative response (143RU). Consequently, when employing the label-free sandwich technique for antibody collocation, the most effective antibody pair for the detection of nucleocapsid proteins was found to be R001 and 7B9.

By choosing a 96- or 384-well plate for application research, we can immobilize proteins on 96 or 384 wells, respectively, at the same time, and then carry out the detection of 96 or 384 samples, respectively. By adding samples only once, the molecular interactions between 96 or 384 samples, respectively, and immobilized proteins can be detected, therefore, the MetaSPR molecular interactions platform has the advantage of providing a high-throughput method (96- or 384-throughtput), especially compared with the traditional SPR single needle injection or 8-channel assay, we have the advantage of high-throughput (96- or 384-throughput).

2.3.5. Application 5: Quantitative Detection

The potential for reinfection by SARS-CoV-2 variants of vaccinated individuals is contingent upon the sustained efficacy of vaccines and the extent of neutralizing antibodies produced against these variants.[32] Consequently, the quantitative assessment of neutralizing antibodies is crucial for evaluating SARS-CoV-2 vaccine efficacy and determining the necessity for a booster shot. In this study, we have devised an innovative nanostructure-coupled nano-plasmonic sensor platform that enables the swift and efficient quantification of the SARS-CoV-2 nucleocapsid protein in a single step. Compared with the method reported in our previous work,[18c] here we immobilized the coated antibody and vacuum-dried AuNPs labeled with the detection antibody on the surface

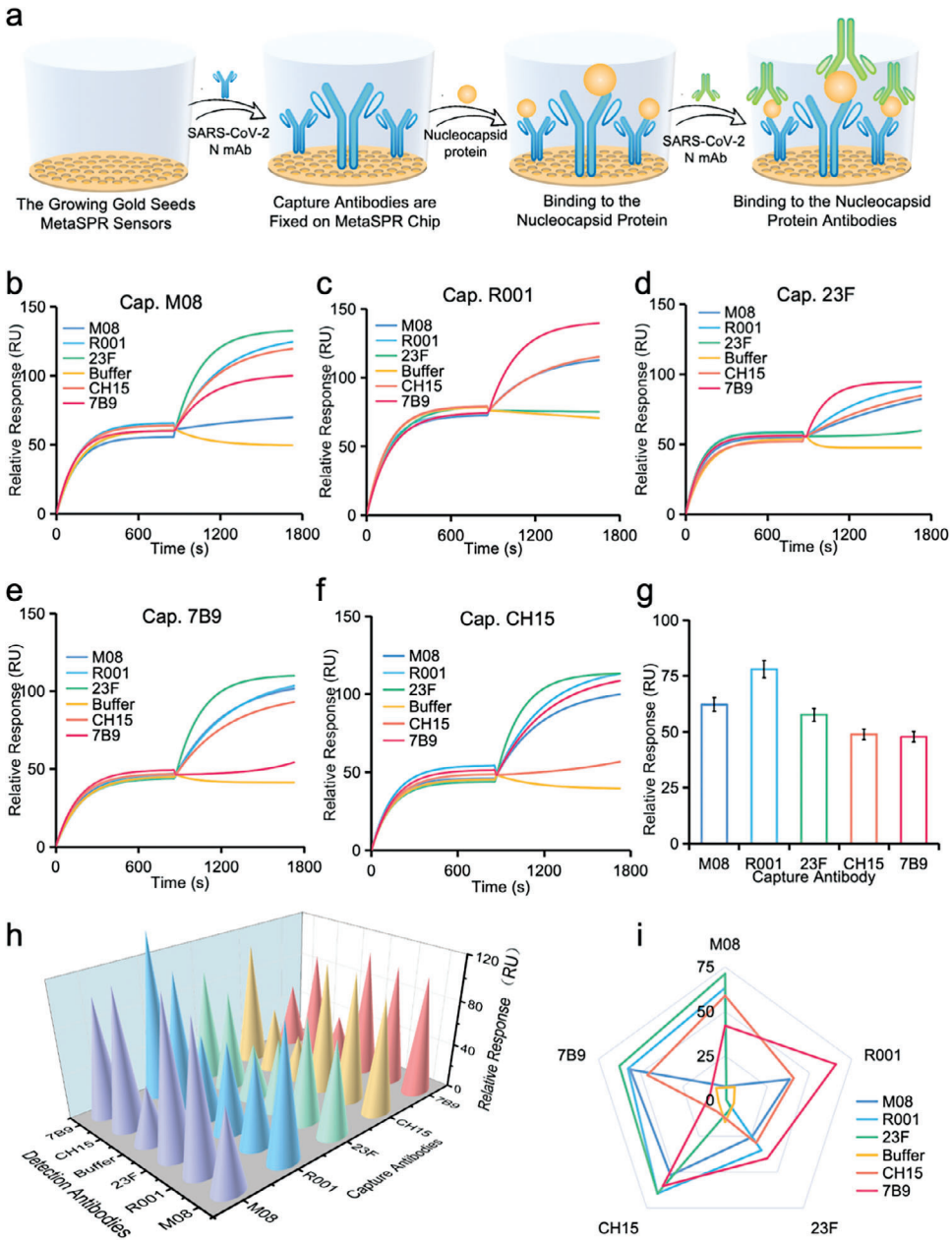

Figure 7. Label-free detection antibody collocation and applications based on the MetaSPR platform. a) Principle and process of antibody collocation are illustrated. b–f) M08, R001, 23F, 7B9, and CH15 were used as the capture antibodies, incubated with nucleocapsid protein and used to detect the relative response results of different nucleocapsid protein specific antibodies. g) Comparison of the binding ability among five capture antibodies and nucleocapsid proteins. Data represent as mean ± SD ($n = 3$). h) Results of the five antibody pairings to detect nucleocapsid protein. i) Comparison of the binding ability between the five antibodies and nucleocapsid proteins.

of the chip. This detection method was named meta-surface plasmonic immunosorbent assay (MetaPISA).

The detection antibody, which was labeled with colloidal gold particles, was subjected to vacuum drying on the chip surface that had been previously treated with the capture antibody. Following the addition of the antigen, the nucleocapsid proteins present in the samples were rapidly quantified using a one-step method. The detection process is visually represented in **Figure 8a**. The antibody pair R001 and 7B9, specifically selected through antibody collocation, was employed. The R001 antibody was immobilized onto the gold chip, while the SARS-CoV-2 N antibody (7B9) labeled with AuNPs was subjected to vacuum drying on the chip surface. The double-antibody sandwich system was employed by introducing the SARS-CoV-2 nucleocapsid protein, and the quantitative detection of the nucleocapsid protein in the sample was achieved using the one-step method. The MetaPLSA system enabled the quantification of low concentrations of the SARS-CoV-2 N protein (0–10 ng mL^{-1}) in the samples. The absorption

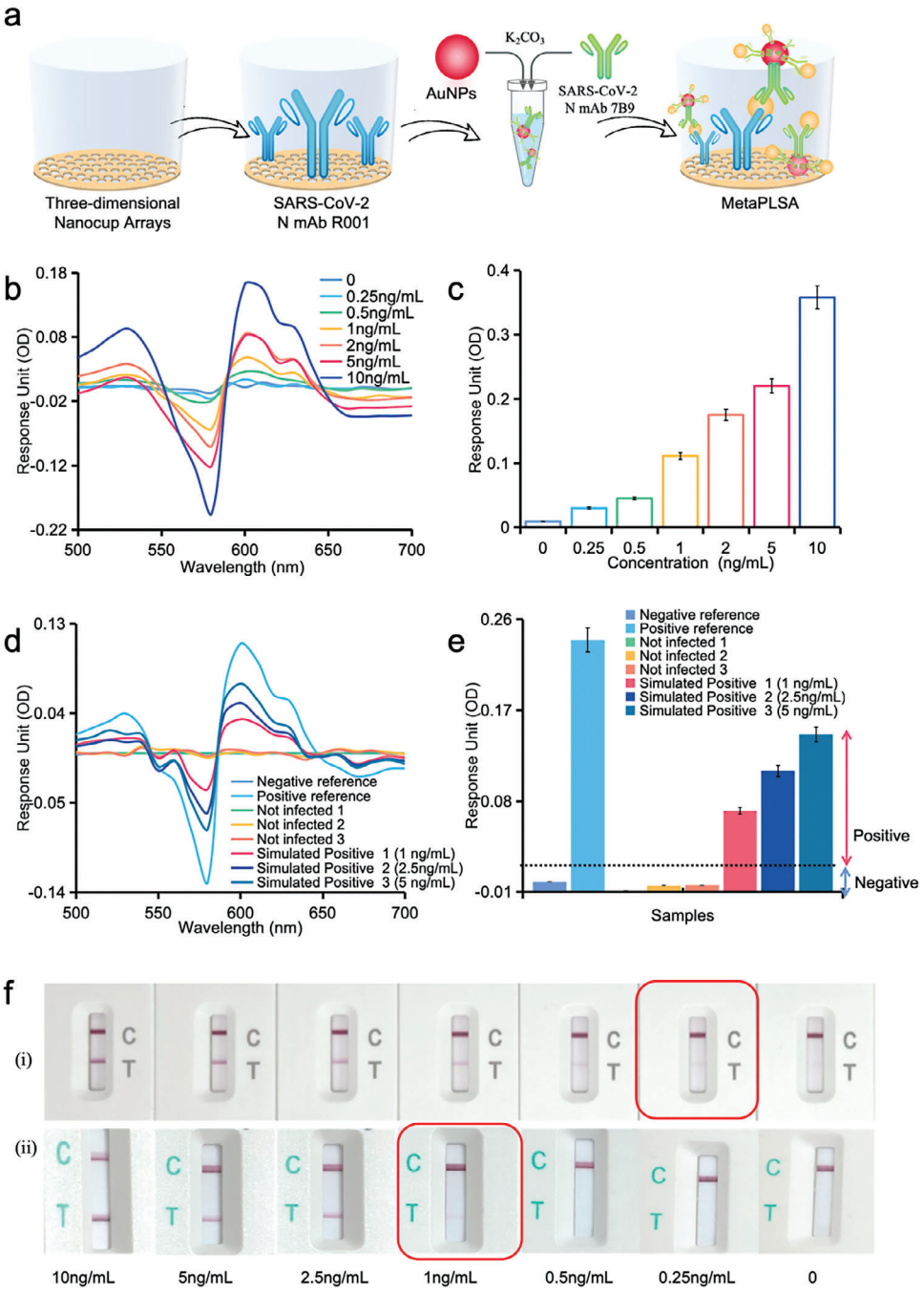

Figure 8. Nano-enhanced quantitative detection methods and applications based on the MetaSPR platform. a) Nano-enhanced MetaPLSA detection. b) Detection of dual-wavelength differences in nucleocapsid proteins by nano-enhanced MetaPLSA detection. c) MetaPLSA system used to verify the sensitivity of the antibody pairs for quantitative detection. Data represent as mean ± SD ($n = 3$). d) Detection of dual-wavelength differences in the throat swab samples of simulated SARS-CoV-2 infections using MetaPLSA. e) Selectivity of the MetaPLSA detection assay for six samples from three not-infected and three simulated-positive infected individuals. Data represent as mean ± SD ($n = 3$). f) Verification of SARS-CoV-2 nucleocapsid protein antibody sensitivity using the colloidal gold method. i) Sensitivity of the colloidal gold strip bound to the antibody pair screened with the MetaPLSA method. ii) Sensitivity of the colloidal gold strip bound to an antibody pair not screened using MetaSPR.

spectra of the wells containing varying concentrations of the SARS-CoV-2 N protein exhibited a noticeable gradient (Figure 8b). The AuNP-coupled MetaPISA demonstrated a limit of detection below 250 pg mL^{-1} for the SARS-CoV-2 N protein (Figure 8c).

The aforementioned detection system was employed to assess simulated samples in order to validate the precision of label-free antibody collocation and the sensitivity of the nano-enhanced detection method. Throughout the experiment, the diluent was designated as the negative reference, while the nucleocapsid protein

served as the positive reference. To ascertain the reliability of the antibody pairs, throat swabs collected from three healthy individuals, as well as throat swab samples containing nucleocapsid protein concentrations of 1, 2.5, and 5 ng mL^{-1}, were used. The findings of this study indicate that the positive reference and simulated positive samples exhibited alterations in dual-wavelength measurements at 575 and 595 nm, while the negative reference and negative samples did not demonstrate any changes in dual wavelength measurements (Figure 8d). The spectral difference results showed that by using 10% of the positive control as the cutoff value, the negative and positive samples were detected as true negative and true positive, respectively (Figure 8e). The"n" value for each data set corresponds to the number of samples analyzed, with "$n = 3$" for both the negative and positive sample groups, indicating that each sample was tested in triplicate to ensure the reproducibility of the results.

Subsequently, we proceeded to fabricate colloidal gold cards using carefully selected antibody pairs and juxtapose them against commercially procurable colloidal gold cards (fabricated using antibody pairs devoid of screening via our technical platform) for the purpose of detecting varying concentrations of nucleocapsid protein. By means of a sensitivity comparison, we aimed to illustrate the consequentiality of screening predicated on Meta SPR sensors. The results indicated that the sensitivity of the colloidal gold strip, which was bound with an antibody pair screened through the MetaPLSA method, was measured at 0.25 ng mL^{-1}. Conversely, the colloidal gold strip bound with an antibody pair that did not undergo screening using this method exhibited a sensitivity of 1 ng mL^{-1} (Figure 8f). This finding offers compelling evidence that the MetaPLSA method exhibits significant promise in the identification of optimal antibody pairs and possesses boundless potential for colloidal gold strip-based detection. Consequently, it is anticipated that this method will make valuable contributions to the advancement of in vitro diagnostics (IVD) technology in the foreseeable future. The utilization of colloidal AuNPs as signal amplifiers for the SPR signal generated by the MetaSPR chip sensor substantially enhances the detection sensitivity. Notably, the MetaSPR sensor can be regenerated approximately ten times using PBS, thereby establishing it as a reproducible and cost-effective detection platform for molecular interactions.

3. Conclusion

This study aims to address the constraints associated with the detection throughput and cost of current SPR sensors. To overcome these limitations, we have developed a novel MetaSPR chip with multiple metal layers and incorporated distinctive surface nanostructures to fabricate novel MetaSPR high-throughput biosensors with 96- and 384-well. Through biochemical modifications, we have successfully manufactured a range of functional sensors. Additionally, we have proposed diverse molecular interaction analysis techniques, such as direct capture, sandwich, and competition, to enhance the capture efficiency and detection sensitivity of the biosensor. Consequently, our approach offers a cost-effective and rapid high-throughput screening solution. Based on the integration of these methodologies, we have successfully devised a range of applications encompassing antibody subtype identification, affinity evaluation, epitope binding, antibody collocation, and quantitative detection. These applications have been employed to assess the feasibility of the MetaSPR platform. Our research is deemed noteworthy within the scientific community as it introduces a groundbreaking technology, MetaSPR, which holds substantial implications for the advancement of biomolecular interaction studies and pharmaceutical development.

Moreover, we have devised a novel MetaPLSA approach by leveraging optimal antibody pairs identified through the utilization of the MetaSPR chip in conjunction with a detection system that exploits colloidal gold particles to enhance the signal and elevate the detection threshold to the picogram range. Consequently, we have successfully validated the MetaSPR platform's efficacy, precision, and sensitivity. As technological advancements continue to unfold, we anticipate enhancing this platform into a high-throughput drug screening system, thereby maximizing its worth and versatility.

4. Experimental Section

Materials: Recombinant protein G was purchased from Biodragon Inc. SARS-CoV-2 nucleoprotein/NP antibodies (N antibodies) R001, M08, and M05 were purchased from Sino Biological Inc; CH15 and CH14 were purchased from Solarbio Inc; 23F and 6F5 were purchased from Easy Biotech Inc.; and 7B9 was purchased from OriGene Inc. SARS-CoV-2 nucleoprotein/NP antigen (N protein) (cat.: RM1033) was purchased from ChunLei JieChuang Bio Inc. The WeSPR200 versatile molecular detector assay system was provided by Liangzhun (Wuhan) Inc. Polyethylene terephthalate (PET) films were purchased from Yixing Yangguang Plastic Co. Ltd. (Yixing, China). A subtype identification kit (ELISA method, used as a control) was purchased from Biodragon Inc. A SARS-CoV-2 Ag rapid detection box (colloidal gold card for comparison) was purchased from Beijing Jeyle Biotech Co., Ltd. Tetrachloroaurate hydrogen trihydrate ($HAuCl_4.3H_2O$, 99.9%), 11 mercaptoundecanoic acid (MUA), 1-(3-dimethylaminopropyl)−3-ethylcarbodiimide hydrochloride (EDC), NTA, L-cysteine (L-Cys), bovine serum albumin (BSA), and ethanolamine were purchased from Sigma Aldrich. $NiCl_2$ and *N*-hydroxy succinimide (NHS) were purchased from Macklin Inc. Ethanol, HCl, and NaOH were purchased from Nanjing Chemical Reagent Co., Ltd. PEG 20 000 (PEG, MW, 20 000) was purchased from Sinopharm Chemical Reagent Co., Ltd. All chemicals were used without further purification.

Preparation and Surface Characterization of the MetaSPR Chip: The biosensor fabrication process employed the replica-molding technique, as outlined in the previous reports.[18c,f] The MetaSPR chip, comprising a conical nanocup array measuring 400 nm in period, 500 nm in height, and 200 nm in upper diameter, was fabricated through nanoindentation and vacuum electroless plating. The formation of conical nanocup arrays on the mold to obtain the initial mold involved laser interference lithography and ion etching. The hydrophobic molds were subjected to a 12-h drying period prior to the reprinting process. Following this, a uniform application of UV light-curing glue was spread onto the mold, and PET sheets were subsequently positioned on the mold. Upon exposure to UV irradiation, a PET film featuring a 3D nanostructure was produced. Subsequently, a sequential deposition of 15 nm Ti, 70 nm Ag, and 20 nm Au[33] was achieved through vacuum electroless plating onto the surface of the nanocup microarray (Figure S4, Supporting Information). The sheet was then cut into 13 cm × 8.5 cm sections and glued to a generated open-bottom 96- or 384-well plate (Figure S5, Supporting Information).

Preparation of the Carboxylation Chip Sensor: The MetaSPR chip was cleaned with a 50 mM NaOH solution, 50 mM HCl solution, 50% ethanol solution, and ddH_2O sequentially before any chemical modification. Organic pollutants and impurities, such as dust from the gold chip surface, were washed away with alcohol. The sensor chip was then immersed in 1 mM MUA solution overnight to form a self-assembled monolayer (SAM). The SAM-functionalized chip was rinsed with the SAM solvent

(ethanol + acetic acid), ethanol, and pure water and stored at 4 °C for later use.

Preparation of the Protein G and NTA Biosensor Chip Sensor: The specific preparation method was as follows: i) after the chip was cleaned, protein G was diluted with CBS buffer to 20 μg mL^{-1}; ii) the sample (2 μL $well^{-1}$) was placed on the surface of the microplate chip, which was maintained at 4 °C for 16 h; iii) protein G was coated onto the surface of the gold chip by physical adsorption; iv) 1% BSA solution was used to block the chip surface at 37 °C for 30 min to avoid non-specific binding; v) the remaining blocking solution was shaken off and a PBS solution containing 5% sucrose was added as a protective agent to prevent degradation of protein G on the chip surface. To avoid the oxidation of the metal chip surface, the chips were stored under vacuum at 4 °C for later use. An NTA MetaSPR sensor was used to capture His-tag molecules. The specific operation process was as follows: the chip was cleaned, and then, 2 μL of NTA (at 20 μg mL^{-1}) was added to the chip well and maintained at 4 °C for 16 h. Then, the chips were dried and stored. The NTA chips must be chelated with Ni ions before use. The chip surface was washed with water, and then, the chip was used to couple His-tagged proteins after 15 min of incubation with 5 mM $NiCl_2$.

Preparation of Chip Sensors with Growing Gold Seeds: The seed gold growth method for chip surface modification was selected based on the modified Turkevich/Frens reaction system.[34] Solutions of L-cysteine and chloroauric acid (0.1–1.0 mM) were diluted with deionized water and combined at a 1:1 ratio for gold seed growth. Specifically, 32 μL of L-cysteine and 40 μL of chloroauric acid, both at the same concentration, were successively injected into each chip well. The chips were then incubated at 25 °C for 30 min. The chips underwent a double wash with deionized water, were subsequently dried using nitrogen gas, vacuum-formed, and stored at a temperature of 4 °C. Following this, the chip was brought back to room temperature and coated with a concentration of 20 μg mL^{-1} of the capture antibody, which was appropriately diluted in carbonate buffer. The chip was then incubated at a temperature of 4 °C for a duration of 16 h. Subsequently, the chip underwent a double wash with deionized water and was subsequently blocked using a 100 μL solution of 1% BSA for a period of 1 h at a temperature of 37 °C. Following the blocking process, the chips were stored at a temperature of 4 °C for future utilization.[18c]

Subtype Identification: Carboxylation MetaSPR sensors were used for subtype identification. The chip was washed twice with deionized water; then, the carboxy groups were activated by adding NHS and EDC to the chip wells, followed by incubation at 37 °C for 15 min. Then, rabbit anti-mouse IgG1, IgG2a, and IgG2b antibodies were diluted with MES (pH, 4.5) to a concentration of 25 μg mL^{-1}; 2 μL of the samples were added to the middle of the chip and covalently attached to the chip surface. Ethanolamine solution was used to inactivate the carboxyl groups, and the remaining sites were blocked with 0.05% fish gelatin and 1% BSA, which reduced non-specific binding to the chip and residual NHS. After blocking, the subtyping identification chip sensor was completed. When identifying the subtypes, the IgG1, IgG2a, and IgG2b subtype antibodies were diluted to a concentration of 20 μg mL^{-1} with HEPES buffered saline (HBS-ET) diluent. Meanwhile, a diluent without antibodies was used as a control; 50 μL of this control solution was added for real-time online detection. The reaction time was set to 10 min, and the response value reading time was set to every 15 s, with each vibration lasting 3 s at a vibration rate of 700 rpm.

Affinity Evaluation: Prior to performing the affinity assay, IgG solutions were introduced into wells on a conventional microplate. Subsequently, 50 μL of IgG analytes (ranging from 0.63 to 100 nM) in HBS-ET buffer were simultaneously introduced into the protein-G-modified MetaSPR chip wells using a multichannel pipette. The association duration was assessed for a period of 10 min using the WeSPR200 instrument. Following the completion of the association process, 150 μL of HBS-ET buffer was added to the chip wells, and the dissociation dynamic curves were promptly monitored. HBS-ET buffer was employed as a control to ascertain the absence of non-specific binding. Subsequently, a 1:1 binding analysis was conducted utilizing XLement Data Analysis software (WeSPR200 1.0.2) to estimate the dissociation constant (KD) of IgG in its interaction with protein G.[16]

Epitope Binding: NTA MetaSPR sensors were used for epitope identification. After processing with NiCl2, SARS-Cov-2 N antibody diluted with CBS (7B9, 15 μg mL^{-1}) was added to the NTA chip sensor and incubated for 10 min. The remaining binding sites were blocked with 1% BSA, which reduced non-specific binding to the chip. For epitope identification, SARS-Cov-2 N protein (RM1033) was diluted to 10 μg mL^{-1} with PBS, bound with various N antibodies (20 μg mL^{-1}) outside the wells for ≈10 min until saturation, and then added to chip wells. The reaction proceeded for 10 min to distinguish antibodies with different epitopes from those for 7B9.

Antibody Collocation: Using the chip sensor of growing gold seeds, SARS-Cov-2 N antibodies were diluted to 20 μg mL^{-1} with CBS diluent, and the 2 μL of each antibody were added separately in different wells of the MetaSPR sensor surface and incubated for 16 h. Then the remaining binding sites were closed with 1% BSA to prevent nonspecific adsorption. Prior to the experiment, vacuum drying was conducted. The nucleocapsid protein was diluted with phosphate-buffered saline (PBS) to a concentration of 7.5 μg mL^{-1}, and subsequently, a 50 μL aliquot of this solution was applied to the chip surface for a duration of 15 min to facilitate association. The liquid within the cavity was discarded, and the plate was subjected to two washes with PBST. Subsequently, 50 μL of distinct N antibody solutions, which had been previously diluted to a concentration of 5 μg mL^{-1} with PBS, were introduced and allowed to react for 15 min. The entire detection process was monitored and recorded.

Quantitative Detection: Quantitative detection was performed using a chip sensor for growing gold seeds and SARS-CoV-2 N antibody (R001) diluted to 25 μg mL^{-1} with CBS diluent. The antibody was immobilized on the surface of the chip and then the remaining binding sites were closed with 1% BSA. Next, 10 μL colloidal-AuNP-labeled SARS-CoV-2 N antibody (7B9) was added and dried on the chip surface under vacuum. The method used for colloidal gold firing and labeling antibodies has been reported in the previous work.[18c] For testing, 50 μL diluted N protein solution (0.25–10 ng mL^{-1}) was added to the chip well to form a MetaPLSA system, and the antibody could be paired in one step. Pharyngeal swabs from healthy individuals were used as negative samples. Dilutions of SARS-CoV-2 N protein (1, 2.5, and 5 ng mL^{-1}) was obtained from the saliva of healthy individuals as mock positive samples. Then the sampled pharyngeal swab sticks were placed in 3 mL of PBS buffer containing 1% BSA, 1% PEG6000, and 1% Tween20. For validation, 50 μL swab solution was added to the chip well, and the changes in resonance were recorded after 10 min of reaction.

Statistical Analyses: Data points in the charts represent individual measurements. For bar graphs with error bars, the indicated values are the mean from three independent experiments ($n = 3$). Error bars represent the standard error of the mean (SEM), calculated as the standard deviation divided by the square root of the sample size (n). The SEM quantifies the variability within each group and facilitates the comparison of the precision of the estimates. Statistical analysis was performed using Origin 2021 software.

Supporting Information

Supporting Information is available from the Wiley Online Library or from the author.

Acknowledgements

Y.C. and H.Z. contributed equally to this work. This work was supported by grants from the Major Program (JD) of Hubei Province (2023BAA011), the Fundamental Research Funds for the Central Universities (2021XXJS112), the National Natural Science Foundation of China (82003305), the Fundamental Research Funds for the Central Universities (YCJJ20241402), and the Major Project of Guangzhou National Laboratory (GZNL2023A03006).

Conflict of Interest

The authors declare no conflict of interest.

Data Availability Statement

The data that support the findings of this study are available from the corresponding author upon reasonable request.

Keywords

drug screening, epitope identification, molecular interaction, surface plasmon resonance sensor

Received: March 23, 2024
Revised: May 23, 2024
Published online:

[1] A. Saftics, S. Kurunczi, B. Peter, I. Szekacs, J. J. Ramsden, R. Horvath, *Adv. Colloid Interface Sci.* **2021**, *294*, 102431.
[2] L. Sarcina, G. F. Mangiatordi, F. Torricelli, P. Bollella, Z. Gounani, R. Österbacka, E. Macchia, L. Torsi, *Biosensors* **2021**, *11*, 180.
[3] D. J. Bornhop, M. N. Kammer, A. Kussrow, R. A. Flowers 2nd, J. Meiler, *Proc. Natl. Acad. Sci. U. S. A.* **2016**, *113*, E1595.
[4] D. Yang, A. Singh, H. Wu, R. Kroe-Barrett, *Anal. Biochem.* **2016**, *508*, 78.
[5] S. K. Singh, S. Singh, R. Singh, *J. Ovarian Res.* **2021**, *14*, 126.
[6] E. Fabini, G. M. Fiori, D. Tedesco, N. P. Lopes, C. Bertucci, *J. Pharm. Biomed. Anal.* **2016**, *125*, 433.
[7] E. E. Bedford, J. Spadavecchia, C. M. Pradier, F. X. Gu, *Macromol. Biosci.* **2012**, *12*, 724.
[8] R. Li, Y. Zhao, H. Fan, H. Zhou, S. Yin, Q. Zhang, M. Jin, G. L. Liu, L. Huang, *Adv. Funct. Mater.* **2023**, *33*, 2306145.
[9] L. P. Hackett, A. Ameen, W. Li, F. K. Dar, L. L. Goddard, G. L. Liu, *ACS Sens.* **2018**, *3*, 290.
[10] R. Li, H. Fan, H. Zhou, Y. Chen, Q. Yu, W. Hu, G. L. Liu, L. Huang, *Adv. Sci.* **2023**, *10*, 2301658.
[11] S. Seo, T. W. Chang, G. L. Liu, *Sci. Rep.* **2018**, *8*, 3002.
[12] A. Ameen, L. P. Hackett, S. Seo, F. K. Dar, M. R. Gartia, L. L. Goddard, G. L. Liu, *Adv. Opt. Mater.* **2017**, *5*, 1601051.
[13] W. Zhang, T. Dang, Y. Li, J. Liang, H. Xu, G. L. Liu, W. Hu, *Sens. Actuators, B* **2021**, *348*, 130711.
[14] W. Hu, T. Dang, Z. Li, L. Lei, G. Wang, Y. Li, H. Xu, Z. Zhou, G. L. Liu, *J. Biomed. Nanotechnol.* **2019**, *15*, 1724.
[15] a) T. Dang, W. Hu, W. Zhang, Z. Song, Y. Wang, M. Chen, H. Xu, G. L. Liu, *Biosens. Bioelectron.* **2019**, *142*, 111494; b) Q. Duan, Y. Liu, S. Chang, H. Chen, J.-h. Chen, *Sensors* **2021**, *21*, 5262.
[16] H. Fan, L. Huang, R. Li, M. Chen, J. Huang, H. Xu, W. Hu, G. L. Liu, *Adv. Funct. Mater.* **2022**, *32*, 2203635.
[17] R. Li, H. Fan, Y. Chen, J. Huang, G. Liu, L. Huang, *Opt. Express* **2023**, *31*, 21586.
[18] a) H. Fan, R. Li, Y. Chen, H. Zhang, S. Zeng, W. Ji, W. Hu, S. Yin, Y. Li, G. L. Liu, L. Huang, *Biosens. Bioelectron.* **2024**, *248*, 115974; b) L. Huang, L. Ding, J. Zhou, S. Chen, F. Chen, C. Zhao, J. Xu, W. Hu, J. Ji, H. Xu, *Biosens. Bioelectron.* **2021**, *171*, 112685; c) L. Huang, Y. Li, C. Luo, Y. Chen, N. Touil, H. E. Annaz, S. Zeng, T. Dang, J. Liang, W. Hu, H. Xu, J. Tu, L. Wang, Y. Shen, G. L. Liu, *Biosens. Bioelectron.* **2022**, *199*, 113868; d) R. Li, Y. Zhao, H. Fan, M. Chen, W. Hu, Q. Zhang, M. Jin, G. L. Liu, L. Huang, *Mater. Today Bio* **2022**, *16*, 100444; e) Y. Zhao, R. Li, C. Lv, Y. Zhang, H. Zhou, X. Xia, S. Yu, Y. Wang, L. Huang, Q. Zhang, G. L. Liu, M. Jina, **2022**, *10*, 2343; f) T. Zhou, W. Ji, H. Fan, L. Zhang, X. Wan, Z. Fan, G. L. Liu, Q. Peng, L. Huang, *Biosensors* **2023**, *13*, 681.
[19] C. Zhang, Y. Chen, H. Tang, Z.-m. Qi, *J. Mater. Chem. C* **2024**, *12*, 639.
[20] a) B. N. Song, S. K. Kim, J. Y. Mun, Y. D. Choi, S. H. Leem, I. S. Chu, *EBioMedicine* **2019**, *50*, 238; b) U. A. K. Saddozai, F. Wang, M. U. Akbar, L. Zhang, Y. An, W. Zhu, L. Xie, Y. Li, X. Ji, X. Guo, *Front. Endocrinol.* **2021**, *12*, 605797.
[21] R. Marega, N. Desroche, A. C. Huet, M. Paulus, C. S. Pantaleon, D. Larose, P. Arbault, P. Delahaut, N. Gillard, *Sci. Rep.* **2020**, *10*, 18439.
[22] A. Bentall, M. Jeyakanthan, M. Braitch, C. W. Cairo, T. L. Lowary, S. Maier, A. Halpin, B. Motyka, L. Zou, L. J. West, S. Ball, *Am. J. Transplant.* **2021**, *21*, 3649.
[23] K. B. Megha, P. V. Mohanan, *Int. J. Biol. Macromol.* **2021**, *169*, 28.
[24] L. Pantaine, V. Humblot, V. Coeffard, A. Vallée, *Beilstein J. Org. Chem.* **2017**, *13*, 648.
[25] D. Zheng, J. Guo, Z. Liang, Y. Jin, Y. Ding, J. Liu, C. Qi, K. Shi, L. Xie, M. Zhu, L. Wang, Z. Hu, Z. Yang, Q. Liu, X. Li, W. Ning, J. Gao, *Adv. Sci.* **2024**, https://doi.org/10.1002/advs.202401327e2401327.
[26] Y. Peng, N. Du, Y. Lei, S. Dorje, J. Qi, T. Luo, G. F. Gao, H. Song, *EMBO J.* **2020**, *39*, 105938.
[27] B. Zhang, J. Tian, Q. Zhang, Y. Xie, K. Wang, S. Qiu, K. Lu, Y. Liu, *Front. Mol. Biosci.* **2022**, *9*, 2568.
[28] B. Yang, S. J. Lin, J. Y. Ren, T. Liu, Y. M. Wang, C. M. Li, W. W. Xu, Y. W. He, W. H. Zheng, J. Zhao, X. H. Yuan, H. X. Liao, *Int. J. Mol. Sci.* **2019**, *20*, 761173.
[29] a) M. Corrado, E. L. Pearce, *J. Clin. Invest.* **2022**, *132*; b) R. Alcalay, R. Falach, Y. Gal, A. Sapoznikov, T. Sabo, C. Kronman, O. Mazor, *Antibodies* **2020**, *9*, 11.
[30] A. S. Adler, D. Bedinger, M. S. Adams, M. A. Asensio, R. C. Edgar, R. Leong, J. Leong, R. A. Mizrahi, M. J. Spindler, S. R. Bandi, H. Huang, P. Tawde, P. Brams, D. S. Johnson, *Monoclonal Antibodies* **2018**, *10*, 431.
[31] R. Kiseleva, C. F. Greineder, C. H. Villa, E. D. Hood, V. V. Shuvaev, J. Sun, A. M. Chacko, V. Abraham, H. M. DeLisser, V. R. Muzykantov, *PLoS One* **2017**, *12*, e0169537.
[32] S. M. Kissler, C. Tedijanto, E. Goldstein, Y. H. Grad, M. Lipsitch, *Science* **2020**, *368*, 860.
[33] W.-S. Kim, K.-H. Oh, T.-H. Kim, S.-H. Shin, T.-W. Um, J.-H. Koh, M. Kamiko, J.-G. Ha, *J. Nanosci. Nanotechnol.* **2020**, *20*, 3231.
[34] C. Bundschuh, M. Egger, K. Wiesinger, C. Gabriel, M. Clodi, T. Mueller, B. Dieplinger, *Clin. Chim. Acta* **2020**, *509*, 79.

